Mathematical and Computer Modelling 55 (2012) 1691–1704

Contents lists available at SciVerse ScienceDirect

Mathematical and Computer Modelling

journal homepage: www.elsevier.com/locate/mcm

Mathematical modeling of the dynamic exchange of solutes during bicarbonate dialysis

Kodwo Annan *

Department of Mathematics and Computer Science, Minot State University, ND 58707, United States

ARTICLE INFO

Article history:
Received 6 November 2010
Received in revised form 29 October 2011
Accepted 3 November 2011

Keywords:
Bicarbonate
Hemodialysis
Acidosis
Mathematical model
Acid–base

ABSTRACT

Most End-Stage Renal Disease (ESRD) patients receiving dialysis therapy are in a state of constant metabolic acidosis which is associated with high cardiovascular morbidity and mortality. In an attempt to improve the quality and efficacy of ESRD patients suffering from acidosis many experimental approaches have been used to investigate acid–base balance during dialysis sessions. However, these experimental approaches are expensive and time consuming. To reduce acidosis morbidity, a compartmental mathematical model is used in this paper. The model takes into account the exchange of small solutes, bicarbonate (HCO_3^-) and carbon dioxide, across a non-uniform trans-membrane dialyzer. Blood and dialysate flows are simulated using the Navier–Stokes and Darcy equations respectively. Since the trans-membrane (TM) flux would not be uniform, both blood- and dialysate-side equations are coupled with interfacial conditions calculated by Kedem–Katchalsky equations. Numerical results and clinical data are in close agreement within a satisfactory range, thus confirming that mathematical models can predict dialysis operative parameters with accuracy. Numerical results also confirm that acid–base balance for ESRD patients can be achieved during HCO_3^- dialysis therapy. Thus, the model quantifies adequate choice of bicarbonate and electrolyte concentrations to help improve acid–base status of ESRD patients suffering from acidosis. As an investigative framework, the model can also provide a clear insight into other small solute exchanges across the dialyzer membrane.

1. Introduction

Hemodialysis (HD) allows the removal of waste products (uremic toxins) and excess fluids from the blood of end-stage renal disease (ESRD) patients. Waste products are normally removed by diffusion (concentration driven) while excess of water accumulation in the body is removed by convection through ultra-filtration (pressure driven). Normally due to the loss of the native kidney functions, an ESRD patient accumulates acid due to metabolism which causes patient's blood bicarbonate (HCO_3^-) level to decrease below physiological range (28–30 mol m^{-3}). As a result, metabolic acidosis is present in most ESRD patients receiving dialysis therapy. In fact, the cardiac function is affected by metabolic acidosis, and symptomatic hypotension is a major risk factor contributing to high cardiovascular morbidity and mortality in ESRD patients [1–6]. Since many ESRD patients are in a state of constant metabolic acidosis, HCO_3^- is now used as a buffer in the dialysis fluid (dialysate) to correct metabolic acidosis in uremic patients. The HCO_3^- buffer consists of carbonic acid/bicarbonate ions and bicarbonate ion/carbonate ions. The main goal of the buffer is to achieve acid–base correction of patients to the normal physiological blood HCO_3^- range.

However, this correction is always a challenge in clinical and experimental studies since dialysis is not able to perform base regeneration in the same way as the native kidney. Studies have shown that current dialysis therapies appear not to

* Tel.: +1 802 338 5725.
E-mail address: kodwo.annan@minotstateu.edu.

0895-7177/$ – see front matter © 2011 Elsevier Ltd. All rights reserved.
doi:10.1016/j.mcm.2011.11.013

Nomenclature

Symbols	Description (Units)
c_s	Solute concentration (mol/m^3)
$c_{s,b}$	Concentration of solute in blood (mol/m^3)
$c_{s,d}$	Concentration of solute in dialysate (mol/m^3)
D_s	Solute diffusivity (m^2/s)
e	Membrane thickness (m)
J_s	Solute flux (kg/m^2 s)
J_v	Volumetric flux (m^3/m^2 s)
L	Dialyzer length (m)
L_r	Width of raise collar (m)
L_p	Hydraulic permeability (m/s Pa)
N	Number of fibers (-)
P_s	Solute diffusive permeability coefficient (m/s)
$P_{s,b}$	Hydrostatic pressure in blood-side (Pa)
$P_{s,d}$	Hydrostatic pressure in dialysate-side (Pa)
q_b	Blood flow rate (m^3/s)
q_d	Dialysate flow rate (m^3/s)
r	Radial direction (m)
r_b	Radius of the tubular membrane (m)
R	Gas constant (K)
r_d	Dialysate-side radius (m)
s	Solutes (CO_2, HCO_3^-) (-)
u_r	Radial velocity (m/s)
u_z	Axial velocity in blood (m/s)
$u_{z_0,b}$	Inlet average axial velocity in blood (m/s)
$u_{z_0,d}$	Inlet average axial velocity in dialysate (m/s)
z	Axial direction (m)
ε	Replenishment constant (-)
μ	Viscosity (Pa s)
ρ	Density (kg/m^3)
σ	Reflection coefficient (-)

normalize the HCO_3^- concentration in a large percent of ESRD patient population [7–13]. To investigate the determinants of acid–base balance in ESRD patients, Soudan et al. [13] conducted a study from 2003 to 2004 on 44 chronic hemodialysis units in Northeast Ohio. They identified patients aged 18 or older who had a serum albumin of less than 3.7 g/dL and had been on dialysis for at least 9 months. Multivariate analyses were used to determine potential determinants associated with predialysis bicarbonate levels. 30% of the patients were associated with metabolic acidosis. The main determinants of metabolic acidosis among the patients were attributed to protein breakdown and dialysis dose.

Sepandj et al. [9] observed over 70 dialysis patients for HCO_3^- gain using high efficiency HD and concluded that diffusive gradient was the most important determinant of HCO_3^- gain. Sombolos et al. [8] investigated ESRD patient's blood passing through hemodialyzer of 14 dialysis patients and observed that gas transfers from dialysate into blood were responsible for acid–base balance in dialysis patients.

In an attempt to address clinical and experimental discrepancies and/or metabolic acidosis simple compartmental theoretical models have been used. Ramirez et al. [14,15] based their parallel plate Kiil dialyzer models on urea kinetics while Lamberti et al. [16] used water and sodium kinetic modeling. However, Noda et al. [17] were among the first to introduce a theoretical modeling on mass transfer using countercurrent flows. Their proposed model assumed a uniform flow distribution of the hollow fibers. Even though their analysis was quite thorough, they admitted that the assumption of uniform flow distribution would prove unrealistic during actual practice.

Salathe et al. [18] studied kinetics of carbon dioxide solute exchange through compartmental modeling based on acid–base balance. Even though their model accounted for the physical and biochemical processes of acid–base balance, they did not account for convection and diffusion of gases along the dialyzer length. Huang and colleagues, [19], developed an improved quantitative model incorporating convective and diffusive transports. However, they did not account for the consumption of gases across the dialyzer membrane.

Perhaps the most relevant literature to the mathematical modeling studies based on acid–base balance was that of Sargent et al., [20,21] and Heineken et al., [22]. The benefits and risks of Sargent and colleagues' one compartmental models have been described and discussed extensively in many clinical and theoretical articles [23–31]. Heineken et al. [22] used a model based on individual prescription of HCO_3^- dialysate concentration. They demonstrated that individual prescription

Table 1
Reaction constants used in this paper at 297 K.

Constant	Value at 297 K	Unit	Refs.
Reaction constant, k_1	3.7×10^{-2}	s^{-1}	[35]
Reaction constant, k_{-1}	1.4×10^{1}	s^{-1}	[35]
Reaction constant, k_4	8.5×10^{3}	$m^3\, s^{-1}\, mol^{-1}$	[35]
Reaction constant, k_{-4}	2.0×10^{-4}	s^{-1}	[35]
Density of water, ρ_w	1.0×10^{3}	$kg\, m^{-3}$	[36]

of HCO_3^- concentration had strong beneficial effect toward a more normal acid–base level state for patients. However, their acid–base dialysate concentration approach did not consider the exchange process inside the dialyzer system and therefore, failed to predict bicarbonate dynamics over the course of a single HD session. Thus, a more complete model consisting of bicarbonate ion transport and solute exchange across the dialyzer membrane is needed to help address metabolic acidosis in dialysis patients.

This paper proposes a model that takes into account the exchange of bicarbonate ions inside the dialyzer and predicts solute exchange dynamics over the course of one dialysis session, typically 4 h. The model formulation for blood and dialysate compartments incorporates bicarbonate buffering and replenishment. The mechanism of bicarbonate ion dynamics oriented to the simulation of HD under buffering conditions, whereby there is an equilibrium binding of water (H_2O) and carbon dioxide (CO_2), is presented. Blood and dialysate flow distributions are simulated using Navier–Stokes and Darcy's equations respectively. Since high flux membranes are widely used in modern dialyzers with high UF and backfiltration (BF) rates [32], the transmembrane (TM) flux would not be uniform along the dialyzer length as mentioned by Gostoli et al. [33]. Therefore, both blood-side and dialysate-side equations are coupled with interfacial conditions calculated by Kedem–Katchalsky (K–K) equations.

Numerical results from the model agreed well with well observed clinical data. The model gave valuable insight of operative parameters and predicted the HCO_3^- and CO_2 exchange during the HD session. The operative parameters and insight of acid–base dynamics are of greater clinical significance for acidosis to get corrected. As an investigative framework, the model may be used to improve the acid–base status of ESRD patients by an adequate choice of HCO_3^- and electrolyte concentrations in the dialysis fluid.

2. Model formulation and algorithm

2.1. Biochemical reactions

In this paper, consideration was limited to water (H_2O), hydrogen ions (H^+), hydroxyl ions (OH^-), and the carbon dioxide (CO_2)-containing species, CO_2, HCO_3^- and carbonic acid (H_2CO_3). Carbonate ion (CO_3^-) is unlikely to be transported across the membrane to any significant extent because of its charge and amount (<1% of total CO_2, [34]) and therefore neglected. Carbon dioxide exists in four different chemical reactions which are interconnected through Eqs. (1) and (2), [35].

$$CO_2 + H_2O \underset{k_{-1}}{\overset{k_1}{\rightleftharpoons}} H_2CO_3 \underset{k_{-2}}{\overset{k_2}{\rightleftharpoons}} H^+ + HCO_3^- \underset{k_{-3}}{\overset{k_3}{\rightleftharpoons}} H^+ + CO_3^{2-} \tag{1}$$

$$OH^- + CO_2 \underset{k_{-4}}{\overset{k_4}{\rightleftharpoons}} HCO_3^- \tag{2}$$

where $k_{\pm1}$, $k_{\pm2}$, $k_{\pm3}$ and $k_{\pm4}$ are the reaction constants. The uncatalyzed hydration–dehydration of CO_2 given by reaction Eqs. (1) and (2) are slow processes with rate constants given in Table 1 while $k_{\pm2}$ and $k_{\pm3}$ are essentially instantaneous.

Therefore, the main biochemical reaction for our model was the active acidic protons, H^+, from blood which reacted with HCO_3^- to form H_2CO_3 and CO_2. These primary CO_2 diffused back into the blood supplying substrates for the continued generation of HCO_3^- and H^+. In addition, the HCO_3^- formed by the reaction in the dialysate diffused into the blood, thereby accomplishing net absorption of HCO_3^-. The principal features of the bicarbonate absorption process in a dialyzer were shown in Fig. 1.

Since the pH in the dialysate could not decline below 6.0, we assumed that changes in H^+ concentration were insignificant compared with the flux of H^+ across the membrane. Thus, all of the H^+ may be considered to be consumed in titrating the bicarbonate buffer, leaving only CO_2, HCO_3^-, and CO_3^{2-} in the reaction. Therefore, the overall reaction could be reduced to Eq. (3):

$$CO_2 + CO_3^{2-} + H_2O \leftrightarrow 2HCO_3^-, \tag{3}$$

with CO_2 and HCO_3^- buffer terms derived by Suchdeo et al., [37] as Eqs. (4)–(5)

$$B_{CO_2} = -k\left(1 + \alpha\frac{2[CO_3^{2-}]}{[HCO_3^-]}\right)\left([CO_2] - \beta\frac{[HCO_3^-]}{[CO_3^{2-}]}\right), \tag{4}$$

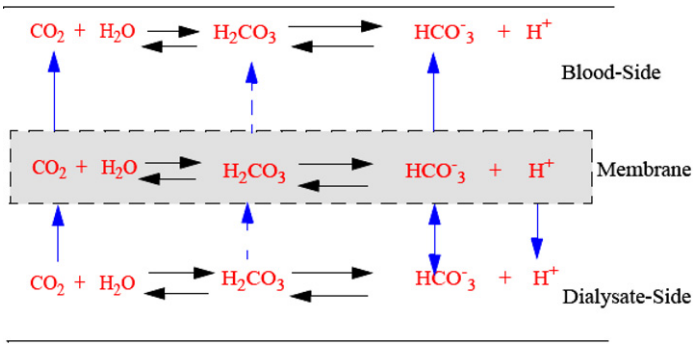

Fig. 1. Principal features of bicarbonate absorption process across the membrane. Solid arrows indicate transport steps playing active role while dashed arrows represents non-significant steps in our model.

and

$$B_{HCO_3^-} = 2k\left(1+\alpha\frac{2[CO_3^{2-}]}{[HCO_3^-]}\right)\left([CO_2]-\beta\frac{[HCO_3^-]}{[CO_3^{2-}]}\right). \tag{5}$$

Here, $\alpha = \frac{k_3K_2}{2k_1K_1}$ and $\beta = \frac{k_{-1}K_1}{k_1}$ were calculated using CO_2 and HCO_3^- reaction constant values in Table 1. The equilibrium constants K_1 and K_2 for the reaction equations $HCO_3^- \overset{K_1}{\rightleftharpoons} H^+ + CO_3^-$ and $H_2O \overset{K_2}{\rightleftharpoons} H^+ + OH^-$ were evaluated using

$$K_1 = \exp\left(-\frac{12092.1}{T} - 36.786\ln T + 235.482\right)\rho_w, \tag{6}$$

and

$$\log K_2 = \frac{1568.9}{T} - 2.5866 - 6.737\times 10^{-3}T, \tag{7}$$

where T and ρ_w are temperature (in Kelvin) and water density, respectively.

Since HCO_3^- concentration was predominant as most carbonic acids dissolved in CO_2, we adapted the Bhagavan [38] ratio for HCO_3^- and H_2CO_3 concentrations, $\frac{HCO_3^-}{[H_2CO_3]} = 20$.

Model mechanism:

In proposing the model, we assumed axial (z) and radial (r) blood and dialysate flows with no tangential direction. The blood-side equations for unsteady incompressible axisymmetric flow in cylindrical coordinate system (r, z) are described by continuity and momentum equations as

$$\begin{aligned}
&\frac{1}{r}\frac{\partial(ru_r)}{\partial r} + \frac{\partial u_z}{\partial z} = 0,\\
&\frac{\partial u_r}{\partial t} + u_z\frac{\partial u_r}{\partial z} + u_r\frac{\partial u_r}{\partial r} = -\frac{1}{\rho}\frac{\partial p}{\partial r} + \frac{\mu}{\rho}\left[\frac{1}{r}\frac{\partial}{\partial r}\left(r\frac{\partial u_r}{\partial r}\right) + \frac{\partial^2 u_r}{\partial z^2} - \frac{u_r}{r^2}\right],\\
&\frac{\partial u_z}{\partial t} + u_z\frac{\partial u_z}{\partial z} + u_r\frac{\partial u_z}{\partial r} = -\frac{1}{\rho}\frac{\partial p}{\partial z} + \frac{\mu}{\rho}\left[\frac{1}{r}\frac{\partial}{\partial r}\left(r\frac{\partial u_z}{\partial r}\right) + \frac{\partial^2 u_z}{\partial z^2}\right],
\end{aligned} \tag{8}$$

where u_r and u_z are velocity components in the radial and axial directions, respectively, p is the pressure, ρ is the constant blood density, and μ is the viscosity. The solute concentration mechanism which is coupled to the velocities is modeled by the convection–diffusion equation

$$\frac{\partial c_s}{\partial t} + u_z\frac{\partial c_s}{\partial z} + u_r\frac{\partial c_s}{\partial r} = D_s\left(\frac{\partial^2 c_s}{\partial r^2} + \frac{1}{r}\frac{\partial c_s}{\partial r} + \frac{\partial^2 c_s}{\partial z^2}\right) + B_s. \tag{9}$$

Here $c_{s,b}$ is the concentration of solute s in blood, B_s denotes the generation rate of the solute, D_s is the constant diffusion coefficient of solute s in the blood.

Since only first derivatives of time exist in Eqs. (8) and (9), it is sufficient to state the initial velocity field at $t = 0$. Using the continuity equation and the fact that flow is driven by pressure gradient in the z-direction with membrane length L and radius r_b, a full developed velocity profile is assumed at the inlet

$$u_z(r) = 2U\left(1-\frac{r^2}{r_b^2}\right) = U_{\max}\left(1-\frac{r^2}{r_b^2}\right), \tag{10}$$

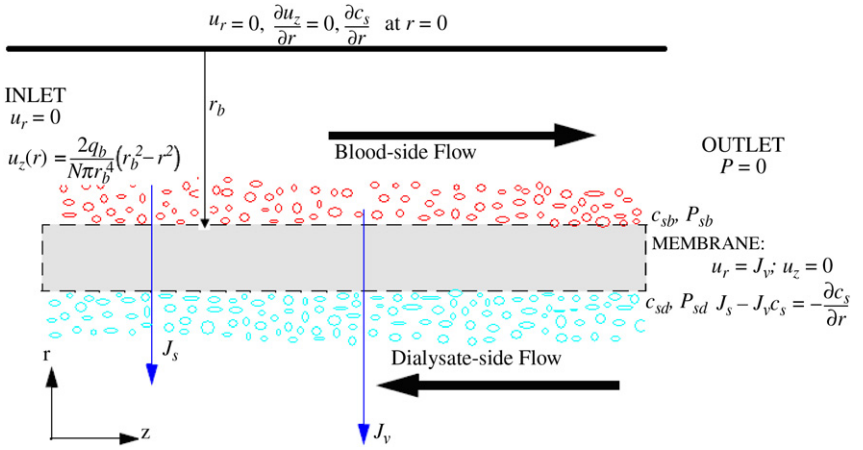

Fig. 2. Mass transport of solutes in blood and dialysate compartments through a single membrane. c_s is solute concentration, while J_v and J_s respectively, indicates blood TM flux and solute TM flux.

where U is the mean velocity and $U_{\max} = u_z(0) = 2U$ is the maximum velocity. For a blood flow rate q_b through a hollow fiber with a fiber cross section area πr_b^2, the inlet velocity conditions for N number of fibers at $z = 0$ and $0 < r < r_b$ are

$$u_r = 0 \quad \text{and} \quad u_z(r) = \frac{2q_b}{N\pi r_b^4}(r_b^2 - r^2). \tag{11}$$

At the outlet where $z = L$ and $0 < r < r_b$, we have

$$u_r = 0 \quad \text{and} \quad \frac{\partial u_z}{\partial z} = 0. \tag{12}$$

Applying no slip and symmetry conditions at the wall and axis of symmetry respectively

$$\begin{aligned} &u_z = u_r = 0. \\ &u_r = 0, \qquad \frac{\partial u_z}{\partial r} = 0 \quad \text{at } r = 0;\ 0 \le z \le L. \end{aligned} \tag{13}$$

The inlet and outlet boundary conditions for the solute concentration equation (9) are

$$c_s(z, r, 0) = c_{s_0}, \qquad c_s(0, r, t) = c_{s_0}, \qquad \frac{\partial c_s(z, 0, t)}{\partial r} = 0. \tag{14}$$

At the membrane surface

$$u_r = J_v, \qquad u_z = 0, \qquad D_s \frac{\partial c_s}{\partial r} = J_v c_s - J_s, \tag{15}$$

where Kedem–Katchalsky equations (i.e. Eq. (16)) calculated the volumetric flux, J_v ($m^3/m^2 s$) and the solute flux J_s (kg/m^2 s) across the dialyzer membrane (Fig. 2).

$$\begin{aligned} J_v &= L_p(P_{s,b} - P_{s,d}) - L_p RT\sigma \Delta c_s, \\ J_s &= C_s^*(1 - \sigma)J_v + P_s \Delta c_s. \end{aligned} \tag{16}$$

Here, L_p (m/s Pa) is the hydraulic permeability of a membrane that describes the volume of blood passing through a membrane area; the solute diffusive permeability coefficient, P_s (m/s), describes the amount of solute passing through the membrane; R is the gas constant; T is the temperature; σ is the reflection coefficient. c_s^* (kg/m^3) represents the average solute concentration at each side of the membrane, Δc_s (kg/m^3) is the difference in solute concentration at each side of the membrane, $P_{s,b}$ and $P_{s,d}$ (Pa) are membrane surface hydrostatic pressure in the blood-side and dialysate-side respectively.

Applying dimensionless forms of variables with respect to the reference length r_b, reference velocity U, and reference concentration c_{s_0}

$$\begin{aligned} &r^* = \frac{r}{r_b}; \quad z^* = \frac{z}{r_b}; \quad u_z^* = \frac{u_z}{U}; \quad u_r^* = \frac{u_r}{U}; \\ &c_s^* = \frac{c_s}{c_{s_0}}; \quad t^* = t\frac{U}{r_b}; \quad p^* = \frac{p}{\rho U^2}; \quad k_{rr}^* = \frac{k_{rr}}{ek_0}; \\ &k_{zz}^* = \frac{k_{zz}}{ek_0}; \quad \mathrm{Re} = \frac{\rho r_b U}{\mu} = \frac{\rho q_b}{\mu r_b}; \quad \mathrm{Pe} = \frac{r_b U}{D_s} = \frac{q_b}{\pi r_b D_s}. \end{aligned} \tag{17}$$

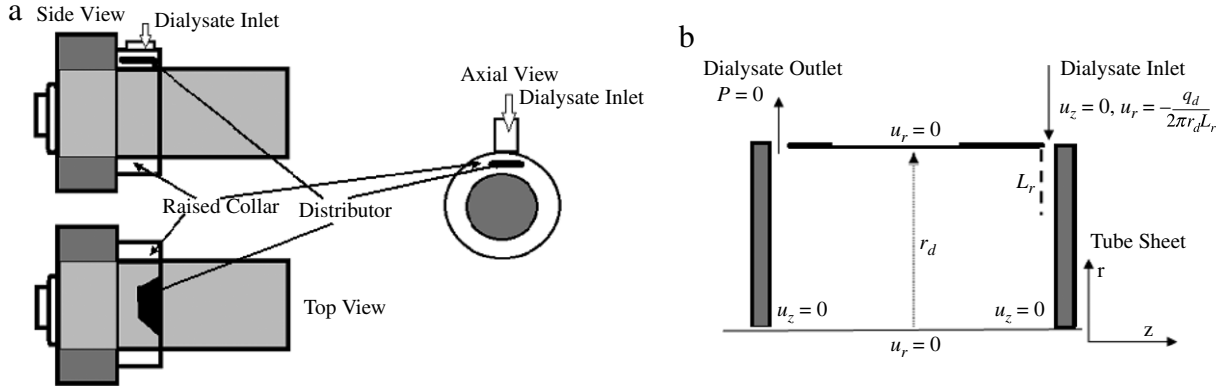

Fig. 3. (a) Geometric configuration near the dialysate inlet. The distributors are designed to keep the dialysate entering the fiber bundle uniform. (b) is the schematic computational domain in the dialysate compartment. The flow distribution is assumed to be uniform in the dialysate inlet and outlet.

Eq. (9) is brought into dimensionless form after dropping the $^*s$

$$\frac{\partial c_s}{\partial t} + u_z\frac{\partial c_s}{\partial z} + u_r\frac{\partial c_s}{\partial r} = \frac{1}{\mathrm{Pe}}\left(\frac{\partial^2 c_s}{\partial r^2} + \frac{1}{r}\frac{\partial c_s}{\partial r} + \frac{\partial^2 c_s}{\partial z^2}\right) + \bar{B}_s. \tag{18}$$

Eq. (18) is characterized by the Reynolds number Re, Peclet number Pe, and the buffer term $\bar{B}_s$. $\mathrm{Re} = \rho U r_b/\mu = \rho q_b/\mu r_b$ relates inertial effects to viscous effects while $\mathrm{Pe} = q_b/\pi r_b D_s$ expresses the relative importance of convection to diffusion. Since dialysis devices employ laminar fluids flow with $\mathrm{Re} \ll 1$ the inertial effects would be irrelevant. Therefore, it will not explicitly appear affecting inertia in the flow equations [39,40].

Contrary to the cylindrical blood flow geometry, a radially-directed fully developed pressure driven dialysate flow in a geometry of radius r_d is assumed. We adapt Frank et al. [41] geometry where a raised collar with a small plate distributor is placed near dialysate inlet and outlet to improve homogeneous distribution in dialysate-side (Fig. 3(a)). The plate distributor prevents the dialysate fluid from entering the fiber bundle directly, thus causing the inlet fluid to impinge on the distributor, then going around the collar before penetrating into the fiber bundle. Similarly, the distributor facing the outlet causes outlet dialysate to first flow out from the fiber bundle and then around the collar before exiting. However, for simplicity our computational domain involves only the plate distributors and the hollow fiber region in between them (Fig. 3(b)).

Based on the above model description, the dialysate flow is treated as the flow in porous media with Darcy equations

$$\begin{aligned}
&\frac{1}{r}\frac{\partial(ru_r)}{\partial r} + \frac{\partial u_z}{\partial z} = 0,\\
&u_r = -\frac{1}{\mu}k_{rr}\frac{\partial p}{\partial r}, \qquad u_z = -\frac{1}{\mu}k_{zz}\frac{\partial p}{\partial z},\\
&\frac{\partial c_s}{\partial t} + u_r\frac{1}{r}\frac{\partial(rc_s)}{\partial r} + u_z\frac{\partial c_s}{\partial z} = R_s,
\end{aligned} \tag{19}$$

where the inlet and outlet boundary conditions at $r = R$; $0 \le z \le L$ are respectively

$$u_r = -\frac{q_d}{2\pi r_d L_r}, \qquad u_z = 0 \quad \text{and} \quad p = 0. \tag{20}$$

The velocity at the tube sheet and initial dialysate solute concentration are

$$u_z = 0 \quad \text{and} \quad c_s(z, r, 0) = c_{s_0}. \tag{21}$$

In Eq. (19), c_s is the solute concentration in dialysate, k_{rr} and k_{zz} are Darcy permeabilities in the radial and axial directions respectively, q_d is the flow rate in the dialysate inlet, L_r is the width of the raised collar, r_d is the dialysate radius, and R_s is the solute replenishment term.

Since there is a tendency for dialysate HCO_3^- concentration to fall below an acceptable level due to low HCO_3^- concentration gradient in the blood, replenishment is introduced to help maintain dialysate HCO_3^- level [13,42]. To simulate fresh bicarbonate into the dialyzer, we use

$$R_s = \varepsilon c_s(c_{s_0} - c_s), \tag{22}$$

where ε is the replenishment coefficient.

Table 2
Geometric and transport characteristics of the hollow-fiber module used.

Parameters	Notation	Value	Refs.
Reflection coefficient	σ	1.0×10^{-4}	[32,45]
Diffusion coefficient of CO_2 in blood ($m^2\ s^{-1}$)	$D_{CO_2,b}$	3.4×10^{-10}	[34,35,37]
Diffusion coefficient of HCO_3 in blood ($m^2\ s^{-1}$)	$D_{HCO_3,b}$	1.4×10^{-10}	[34,35,37]
Diffusion coefficient of CO_2 in dialysate ($m^2\ s^{-1}$)	$D_{CO_2,d}$	1.59×10^{-9}	[34,35,37]
Diffusion coefficient of HCO_3^- in dialysate ($m^2\ s^{-1}$)	$D_{HCO_3,d}$	1.18×10^{-9}	[34,35,37]
Membrane effective length (m)	L	0.22	[32,46]
Hydraulic permeability (m/s Pa)	L_p	1.15×10^{-10}	[32]
Width of raise collar (m)	L_r	0.01	[32]
Fiber diameter (μm)		200	[32,46]
Fiber thickness (μm)	e	40	[46]
Number of fibers	N	9000–12000	F60 Model CT190G
Membrane permeability of CO_2 ($m\ s^{-1}$)	P_{CO_2}	1.72×10^{-9}	[34,35,37]
Membrane permeability of HCO_3 ($m\ s^{-1}$)	$P_{HCO_3^-}$	1.95×10^{-9}	[34,35,37]
Radius of dialysate channel (m)	r_d	1.25×10^{-4}	[46,47]
Radius of blood channel (m)	r_b	2.0×10^{-4}	[46,47]
Initial velocity at blood inlet ($m\ s^{-1}$)	$u_{z_0,b}$	1.73×10^{-2}	[32,46,48]
Initial velocity at dialysate inlet ($m\ s^{-1}$)	$u_{z_0,d}$	1.21×10^{-2}	[32,46,48]
Darcy permeability in radial direction (m^2)	k_{rr}	4.16×10^{-11}	[32]
Darcy permeability in axial direction (m^2)	k_{zz}	1.29×10^{-9}	[32]

2.2. Algorithm and techniques

In delivering an algorithm for the simulation of the dimensionless model equations for (18)–(22), Finite Volume Method (FVM) was used to transform the model systems. Application of FVM resulted in the creation of grid structures such that the number of rectangular cells in the r and z directions remained constant throughout the domain of interest. However, the grid size was made to vary, although strong variations in grid size could affect the accuracy [43]. Since the model equations provided no direct means for pressure–velocity coupling, a semi-implicit method for pressure linked equation (SIMPLE) method was used for pressure coupling.

The velocity distribution was calculated with a Picard iteration method using stabilized bi-conjugate gradients with a tolerance of 10^{-8}. Since the Peclet number was small, the central differencing method was used for its simplicity and accuracy [43]. However, for suspected high Peclet numbers, the hybrid differencing method was used. The method switched to upwind differencing when central differencing produced inaccurate results at high Peclet numbers. The concentration equations were solved using Picard iteration with a tolerance of 10^{-8}. In order to account for the diffusivity differences between the blood and dialysate sides, boundaries of the domain of interest were chosen at the faces of the rectangular control volumes, rather than at its grid points. Therefore, following the approach of Versteeg et al. [43], one extra grid row or column outside the boundary was allowed for an easy application of the boundary conditions in the following order of calculations:

- Transport equations for interior points,
- Left ($z = 0$) and right ($z = L$) boundary conditions in both the blood and dialysate sides, and
- the boundary conditions in both sides of the membrane in any order.

Fig. 4 showed dependences between the boundary conditions with arrows indicating the sequence of application required by the dependences.

Hence, the solution methodology for our model was to solve the dimensionless versions of Eqs. (18) and (19) for pressure, velocity, and concentration distributions in blood and dialysate compartments. Pressure and concentration calculated were then transferred to Kedem–Katchalsky equations as boundary conditions to calculate the TM flux of carbon dioxide and bicarbonate solutes. The TM flux values were used to calculate the replenishment term (R_s) and then used as the boundary conditions in the Navier–Stokes equations to generate the next iteration.

2.3. Model constants

In these simulations, blood and dialysate inlet bicarbonate concentrations were set to 19 mol m^{-3} and 35 mol m^{-3} respectively, while the blood-side and dialysate-side flow rates were respectively, 350 mL/min (i.e. $5.83 \times 10^{-6}\ m^3\ s^{-1}$) and 800 mL/min ($1.33 \times 10^{-5}\ m^3\ s^{-1}$), [7,32,44]. Parameters and constants used in this paper are listed in Table 2. Others not shown in this table were variables or parameters computed using values in Table 2.

3. Results and discussions

Fig. 5 showed concentration distribution of CO_2 in the blood as a function of dialyzer membrane length (L). It was observed that CO_2 concentration initially increased, from 1.40 to 1.57 mol m^{-3}, before decreasing steadily as the axial

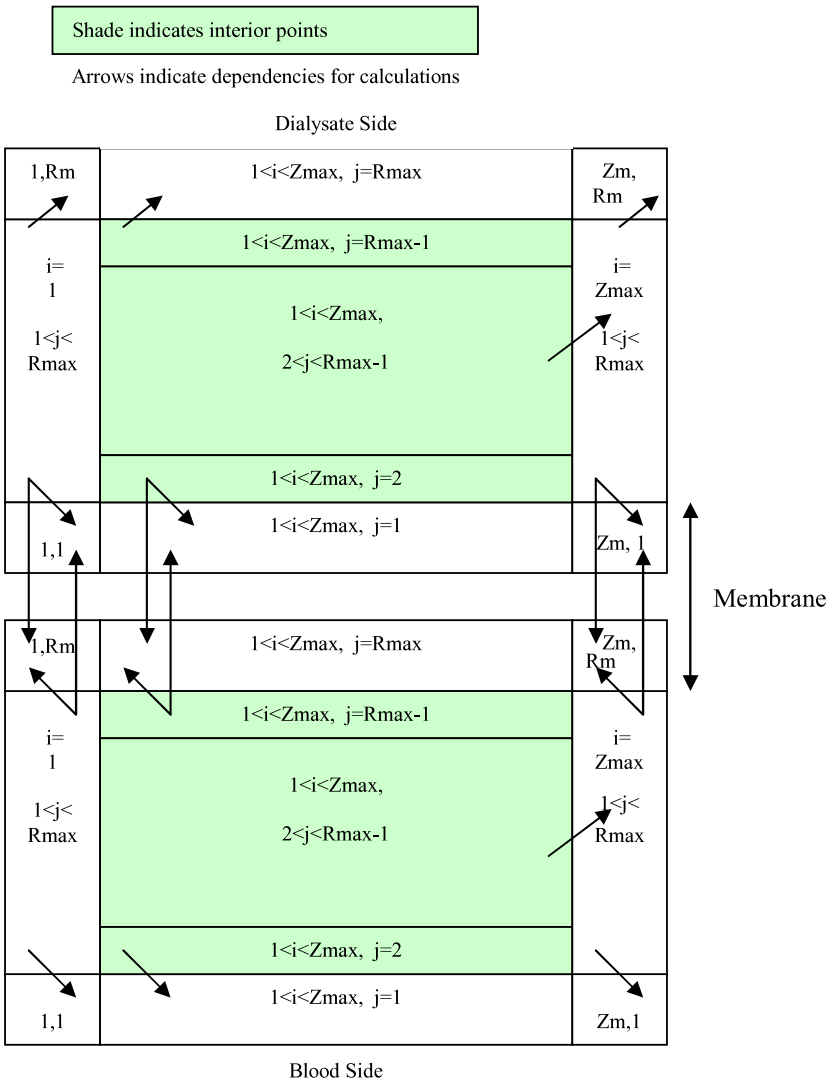

Fig. 4. Dependences between the BCs with arrows, which in turn defines the sequence of application required by these dependences. The BC at the upstream boundary in each side is a constant. All other BCs depend on values in the current time step.

distance increased. The initial CO_2 increase may be caused by (i) active H^+ from blood reacting with HCO_3^- in dialysate to produce more of the primary substances (H_2CO_3 and CO_2), (ii) incomplete dissociation of HCO_3^- into CO_2 in the blood compartment, and (iii) the differences in total CO_2 between blood and dialysate causing some of the dissolved CO_2 to diffuse into the patient blood.

The decreasing trend of CO_2 concentration distribution indicated that most CO_2 solute desorption occurred in the blood. The effective removal of CO_2 from the blood could be explained by the oxygenation of blood facilitated by the respiratory system. Since more than 90% of CO_2 in the blood exists in the form of HCO_3^-, the actual dissolved CO_2 gas in the blood was observed to be about 0.86 mol m^{-3} as shown in Fig. 5.

When dialysis therapy started, HCO_3^- in the dialysate diffused into the blood due to the concentration gradient. Fig. 6 showed HCO_3^- concentration distributions in the blood along the membrane length. The result indicated that the HCO_3^- concentration increased along the dialyzer membrane length. The rate of increase and the degree to which HCO_3^- increased were determined by (i) the immediate buffer response from the dialysis fluid, and (ii) the extent to which organic acid (lactate or acetoacetate) production was increased.

A rapid HCO_3^- concentration increased was observed in the first 2.2 h of the dialysis therapy and then became nearly stable during the remaining time of the treatment. The stability observed in the later stage of the treatment implied that there were no HCO_3^- mass transfer across the membrane. Meaning, the amount of HCO_3^- entering the dialyzer equaled the amount of HCO_3^- leaving the dialyzer. Thus, patient's blood HCO_3^- concentration level reached dialysate HCO_3^- concentration level. Furthermore, a significant increase in the HCO_3^- concentration (about 8.8 mol m^{-3}, from 19.0 to 27.8 mol m^{-3}) between

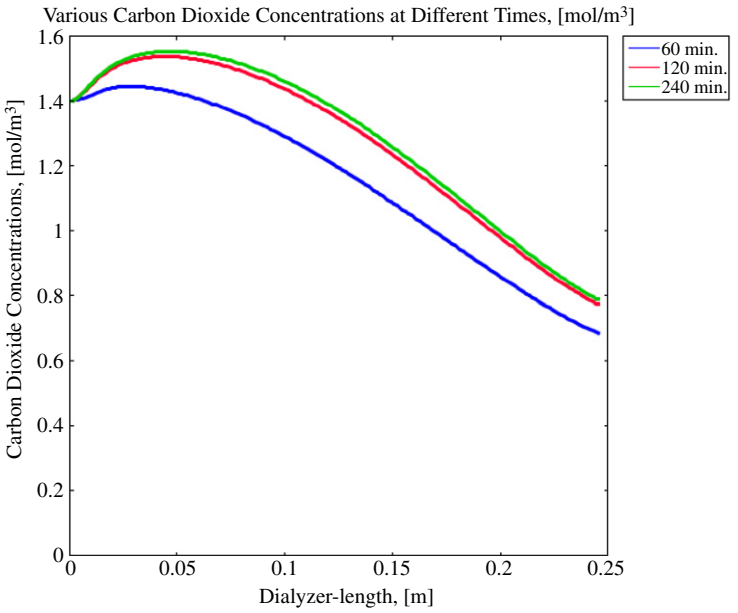

Fig. 5. Graph shows boundary carbon dioxide concentration in the blood at specific values on r against the membrane length (L) after 4 h of dialysis session. The plot shows carbon dioxide concentrations decreasing at specific values of r along membrane length which indicates carbon dioxide desorption in the blood.

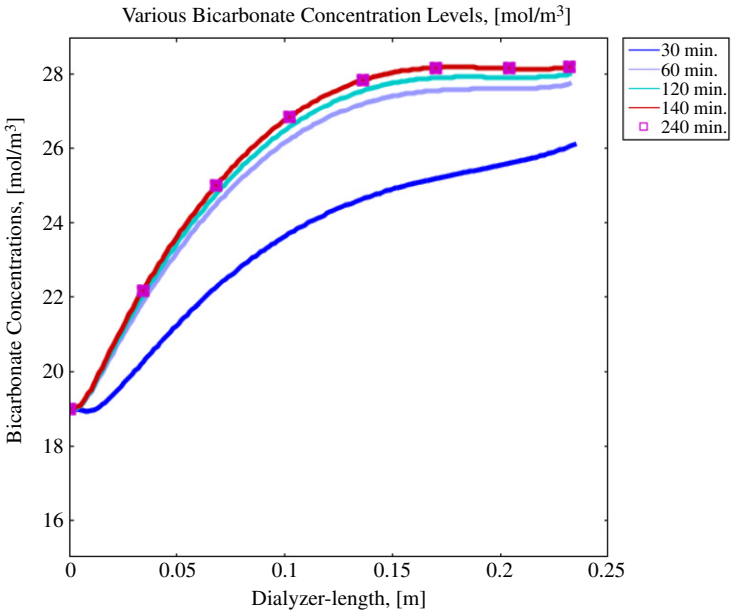

Fig. 6. Graph of various bicarbonate concentrations at different times in the blood along dialyzer membrane length. It indicated that after just 2 h on the dialysis treatment, bicarbonate concentration in the blood almost reached its highest concentration level.

pre- and post- dialysis blood HCO_3^- concentrations was observed. This observation confirmed clinical studies that dialysis patients achieve a stable bicarbonate concentration level (normally between 26 and 30 mol m^{-3}) during a dialysis session [44,49–51].

Comparing blood HCO_3^- concentration results from our simulation with experimental results obtained by Pedrini et al. [52] showed increased HCO_3^- concentration from 19.0 mol m^{-3} to 26.2 mol m^{-3} within an hour and then to 27.8 mol m^{-3} at the end of therapy session. Pedrini et al. reported 19.5–24.3 mol m^{-3} within an hour and then increased slowly to 26.6 mol m^{-3}. Therefore, our model gave a mean HCO_3^- concentration increase of 8.8 mol m^{-3} (i.e. 46.3%) which was higher than the concentration increase obtained by Pedrini et al., 7.1 mol m^{-3}.

Table 3
Experimental and numerical results of HCO_3^- concentrations (mol m^{-3}) for 107 dialysis patients denoted by n.

n	HCO_3^- baseline	Clinical data	Numerical data	Error margin (%)
12	17.0	21.1	24.77	17.4
11	15.6	24.0	24.01	0.04
38	19.0	24.8	25.86	4.3
8	18.6	25.3	25.65	1.4
6	18.5	24.8	25.62	3.3
16	16.7	20.3	24.60	21.8
7	19.3	26.2	26.03	0.6
9	22	25.9	27.50	6.2

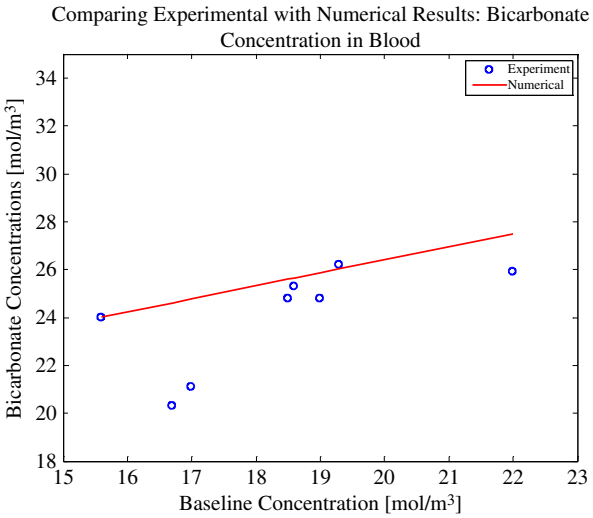

Fig. 7. Plot comparing experimental and numerical results shows that numerical results agree well with experimental results and are within a physiological range after bicarbonate dialysis session.

Table 3 compared clinical data and numerical results of bicarbonate concentrations of 107 patients with blood and dialysate flow rates set at 350 and 800 mL/min respectively.

Patient's pre-dialysis blood HCO_3^- (baseline) was recorded based on three variables: metabolic acid production, ultra-filtration, and the amount of buffer infusion. The dialysis procedure (blood flow, dialysate flow, HCO_3^- dialysate concentration, membrane dimensions) and ultra-filtration were kept constant so that a stable pre-dialysis blood HCO_3^- is recorded [5,51]. The post-dialysis blood HCO_3^- depended on both pre-dialysis blood HCO_3^- and body weight, and the amount of buffer infused with the replacement fluid [53].

Patients showed high-bicarbonate levels for both clinical and numerical studies. The result revealed that high-bicarbonate dialysate corrected pre-dialysis acidosis. The mean numerical and clinical results were within 7% error margin which indicated that numerical results were in good agreement with clinical data.

Fig. 7 compared clinical and numerical bicarbonate concentrations in patient's blood with their baseline concentrations. While numerical results showed a linear relationship between pre- and post-blood HCO_3^- concentrations and were within the physiological range (26–30 mol m^{-3}), the clinical values fell short of the range significantly. The variation may be caused by (i) the diffusion–convection technique considered for the transport mechanism between blood and dialysate or (ii) the physiological aspect of the patient whose data was taken.

To examine the actual CO_2 and HCO_3^- concentrations entering a patient's body we plotted both exit bulk and boundary concentrations in Figs. 8 and 9. The transport of dissolved carbon dioxide solute from bulk concentration (shown in Fig. 8) was observed to be the limiting step in the CO_2 solute exchange process. Since boundary CO_2 concentration was lower than bulk concentration, we expected a complete permeation of CO_2 through the membrane. However, due to the influence of both carbonate and bicarbonate ions on bulk concentration in the exchange membrane, a possible reduction in the CO_2 bulk flux was observed. This difference indicated that dissolved CO_2 in the blood was affected by the dissociation reaction rate of bicarbonate ions in the membrane.

Boundary and bulk HCO_3^- concentration distributions along the dialyzer length were shown in Fig. 9. As observed, the bulk and boundary HCO_3^- concentrations at the exit point of the membrane were almost identical and stable against the dialysis length. This was crucial to verify because the bulk concentration level actually enters the patient's body and might put the patient at risk of bicarbonate overdose if it is not within the physiological range or stable. However, the observed

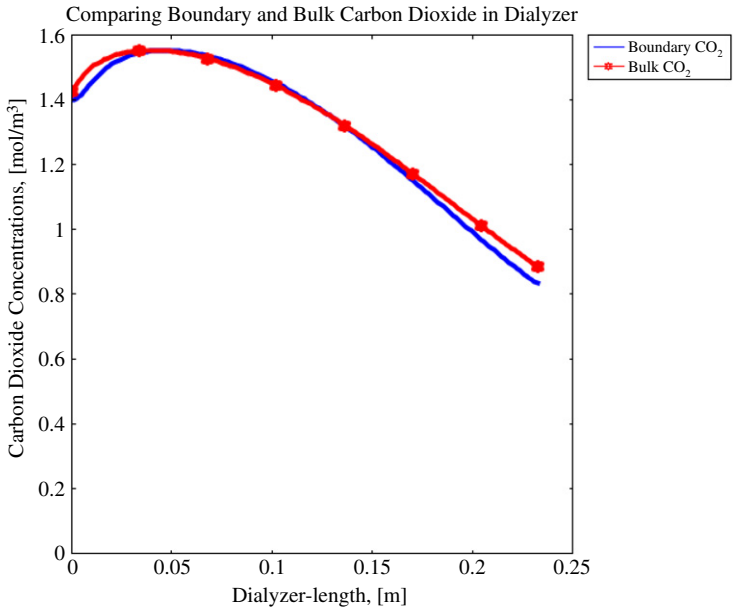

Fig. 8. Shows transient boundary and bulk concentration graphs of carbon dioxide in the blood as a function of dialyzer arc length after 4 h.

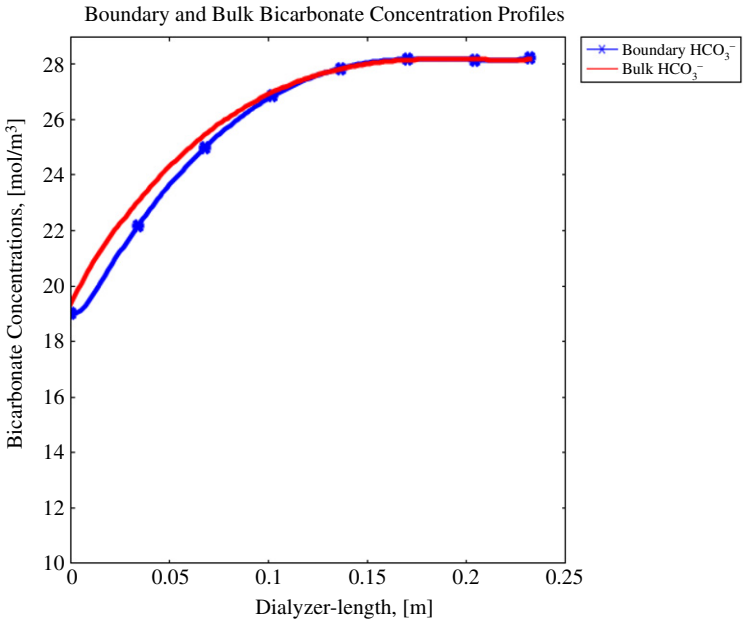

Fig. 9. Graph of boundary and bulk concentration profiles of bicarbonate in the blood as a function of dialyzer length within a dialysis session (for 4 h).

bulk HCO_3^- inlet concentration was not 19.0 mol m^{-3} (initial value), but 19.7 mol m^{-3}. The discrepancy maybe caused by incomplete dissociation of carbonic acid (H_2CO_3) into HCO_3^- and H^+ which resulted in the HCO_3^--ion carryover effect. Nevertheless, our simulation ended with both boundary and bulk HCO_3^- concentrations falling within physiological range (26–30 mol m^{-3}) and significantly more than the pre-dialysis value, (19–27.8 mol m^{-3}).

To investigate the sensitivity of bicarbonate dialysate concentration during the dialysis session, four HCO_3^- dialysate concentrations (30, 35, 40, and 45 mol/m^3) were compared. A dialysate inlet flow rate of 800 mL/min and a CO_2 pressure of 63.6 mmHg (i.e. 1.91 mol m^{-3}) [54] were used. It was observed that HCO_3^- transfer from dialysate to blood depended on dialysate initial HCO_3^- concentration; see Fig. 10. However, there was an unusually high HCO_3^- concentration lost in the dialysis fluid. The amount of HCO_3^- concentration lost in the dialysis fluid could be (i) transferred into the patient's blood (ii) captured inside the dialyzer membrane, and/or (iii) consumed by unexplained phenomena that occurred in the

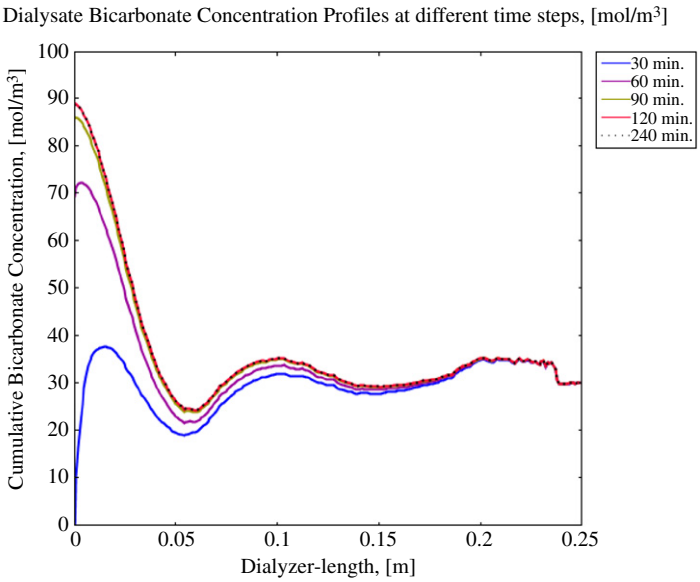

Fig. 10. Graph showing various initial bicarbonate dialysate concentrations as a function of dialyzer length. Even though the concentration distributions are non-uniform, the highest concentration level in most parts of the dialyzer length is below 35 mol m^{-3} and the outlet concentration is within the 27–31 mol m^{-3} (little more than physiological range for ESRD patients).

dialysis fluid. Nevertheless, the exit dialysate HCO_3^- concentration values were within the accepted range. This observation suggested that there may be a better way of quantifying the amount of HCO_3^- concentration lost in the dialysis fluid.

Fig. 10 also suggested that a patient's blood HCO_3^- concentration reached the inlet HCO_3^- dialysate concentration (about 30.6 mol m^{-3}). Even though this value seemed higher than the physiological range, one wondered whether a patient actually experienced post-dialysis alkalosis. However, research suggested that a patient's HCO_3^- concentration level decreases rapidly during few hours after dialysis therapy [49]. Therefore, we may be tempted to use higher initial HCO_3^- dialysate concentration (>35 mol m^{-3}) without risking patient's health. This observation reinforces clinical study suggesting that a new steady-state for higher dialysate HCO_3^- must be investigated further [55].

Also, we expected a monotonic dialysate HCO_3^- profiles as there exist a linear relation between the mass transfer and the concentration gradient. However, the mass transfer decreased faster than the concentration gradient, thus, causing a nonconstant HCO_3^- gradient.

4. Conclusion

Metabolic acidosis is very common in ESRD patients. One of the goals of dialysis treatment is to improve acid–base status of the patient by an adequate choice of bicarbonate in the dialysis fluid. This paper used mathematical model to quantify operative parameters and predicted bicarbonate and carbon dioxide in ESRD patient's blood that could help correct metabolic acidosis. Navier–Stokes and Darcy's equations were employed to simulate blood and dialysate sides, respectively. K–K equations were used to solve trans-membrane flow. Physical parameters such as diffusivity and permeability were obtained from the literature and presented in Tables 1 and 2. Numerical results agreed well with clinical data with an average of 7% error margin.

Numerical results showed an initial CO_2 increase in the blood before decreasing along the dialyzer length. The initial increase was attributed to (i) active hydrogen ions from blood reacting with bicarbonate ions to produce more carbon dioxide and carbonic acid (ii) incomplete dissociation of HCO_3^- into CO_2 in the blood, and (iii) differences in total CO_2 between blood and dialysate causing some of dissolved CO_2 to diffuse into the patient's blood. The rapid CO_2 concentration decrease signified that most of the carbon dioxide were desorbed in the blood. Blood side HCO_3^- concentration curve increased steadily within the first 2.2 h of dialysis session and then remained stable afterward. The stability implied that the amount of HCO_3^- entering the dialyzer equaled the amount of HCO_3^- leaving the dialyzer. Thus, we concluded that dialysis patients achieve a stable bicarbonate concentration level (28–30 mol m^{-3}) during a dialysis session. Sensitivity analysis conducted with various dialysate HCO_3^- concentrations higher than 35 mol m^{-3} resulted in slightly higher than normal blood HCO_3^- level. The model gave valuable insight of operative parameters and predicted HCO_3^- and CO_2 exchange during the HD session. As an investigative framework, the model may be used to improve acid–base status of ESRD patients by an adequate choice of the HCO_3^- and electrolyte concentrations in the dialysis fluid.

Acknowledgments

This work was partially funded through graduate teaching assistantship by the Department of Mathematics and Statistics, University of Vermont. The author also wishes to express his thanks to his graduate advisory committee for their critical evaluation throughout this research.

References

[1] S.M. Hossli, Clinical management of intradialytic hypotension: survey results (continuing education), Nephrol. Nurs. J. 32 (3) (2005) 287–291.
[2] D.V. Vlahakos, K. Retsa, S. Kalogeropoulou, S. Katsoudas, D. Bacharaki, B. Agroyannis, Chronic acid–base perturbations in hemodialysis patients treated with sevelamer hydrochloride: a two-year follow-up study, Artif. Organs 31 (12) (2007) 892–895.
[3] R. Mehrotra, J.D. Kopple, M. Wolfson, Metabolic acidosis in maintenance dialysis patients: clinical considerations, Kidney Int. Suppl. 88 (2003) S13–25.
[4] J. Bommer, F. Locatelli, S. Satayathum, et al., Association of predialysis serum bicarbonate levels with risk of mortality and hospitalization in the dialysis outcomes and practice patterns study (DOPPS), Am. J. Kidney Dis. 44 (2004) 661–671.
[5] F.J. Gennari, Acid–base considerations in end stage renal disease, in: W.L. Henrich (Ed.), Principles and Practice of Dialysis, Lippincott Williams & Wilkins, Philadephia, PA, 2004, pp. 393–407.
[6] J.D. Kopple, K. Kalantar-Zadeh, R. Mehrotra, Risks of chronic metabolic acidosis in patients with chronic kidney disease, Kidney Int. Suppl. 95 (2005) S21–7.
[7] F.J. Gennari, M. Feriani, Acid–base problems in hemodialysis and peritoneal dialysis, in: N. Lameire, R.L. Mehta (Eds.), Complications of Dialysis, Marcel Dekker Inc., 2000, p. 361 (Chapter 19).
[8] K.I. Sombolos, G.I. Bamichas, F.N. Christidou, L.D. Gionanlis, A.C. Karagiani, T.C. Anagnostopoulos, T.A. Natse, pO_2 and pCO_2 in post dialyzer blood: the role of dialysate, Artif. Organs 29 (11) (2005) 892–898.
[9] F. Sepandj, K. Jindal, B. Kiberd, D. Hirsch, Metabolic acidosis in hemodialysis patients: a study of prevalence and factors affecting intradialytic bicarbonate gain, Artif. Organs 20 (9) (1996) 976–980.
[10] P. Chauveau, D. Fouque, C. Combe, Acidosis and nutritional status in hemodialyzed patients: French study group for nutrition in dialysis, Semin. Dialysis 13 (2000) 241–246.
[11] B. Kirschbaum, Effect of hemodialysis on electrolytes and acid–base parameters, Clin. Chim. Acta 336 (2003) 109–113.
[12] K.A. Graham, N.A. Hoenich, M. Tarbit, M. Ward, T.H.J. Goodship, Correction of acidosis in hemodialysis patient increases the sensitivity of the parathyroid glands to calcium, J. Am. Soc. Nephrol. 8 (4) (1997) 627–631.
[13] K. Soudan, E.S. Ricanati, J.B. Leon, A.R. Sehgal, Determinants of metabolic acidosis among hemodialysis patients, Hemodial. Int. 10 (2006) 209–214.
[14] W.F. Ramirez, M.C. Mickley, D.W. Lewis, Mathematical modeling of a Kiil hemodialysis, in: R.G. Buckles (Ed.), Advances in Bioeng, in: Chemical Eng. Symposium Series, 1970, pp. 116–127.
[15] W.F. Ramirez, M.C. Mickley, D.W. Lewis, Characterization of parallel-plate Kiil dialysers, Med. Bioeng. 10 (1972) 267–275.
[16] C. Lamberti, E. Sarti, A. Santoro, M. Spongano, P. Zucchelli, M.A. Rossi, A digital computer model for optimal programming of hemodialytic treatment, Int. J. Artif. Organs 11 (1988) 235–242.
[17] I. Noda, D.G. Brown-West, C.C. Gryte, Effect of flow maldistribution on hollow fiber dialysis—experimental studies, J. Membr. Sci. 5 (1979) 209–225.
[18] E.P. Salathe, R. Fayad, S.W. Schaffer, Mathematical analysis of carbon dioxide transfer by blood, Math. Biosci. 57 (1981) 109–153.
[19] N.S. Huang, J.D. Hellums, A theoretical model for gas transport and acid/base regulation by blood flowing in microwavessels, Microvasc. Res. 48 (1994) 364–388.
[20] J.A. Sargent, F.A. Gotch, Mathematical modeling of dialysis therapy, Kidney Int. 18 (Suppl. 10) (1980) 2–10.
[21] J.A. Sargent, F.A. Gotch, in: J.F. Maher (Ed.), Dialysis Principles and Biophysics of Dialysis in Replacement of Renal Function by Dialysis, Kluwer Academic Publishers, New York, 1989, pp. 87–143.
[22] F.G. Heineken, M. Brady-Smith, J. Haynie, J.C. Van Stone, Prescribing dialysate bicarbonate concentrations for hemodialysis patients, Int. J. Artif. Organs 11 (1988) 45–50.
[23] M. Burgelman, R. Vanholder, H. Fostier, S. Beigair, Estimation of parameters in a two-pool urea kinetic model for hemodialysis, Med. Eng. Phys. 19 (1997) 69–76.
[24] J.D. Kopple, M.R. Jones, P.R. Keshaviah, J. Bergstrom, R.M. Lindsay, J. Moran, K.D. Nolph, A proposed glossary for dialysis kinetics, Am. J. Kidney Dis. 26 (1995) 963–981.
[25] M. Maasrani, M.Y. Jaffrin, M. Fischbach, B. Boudailliez, Urea, creatinine and phosphate kinetic modeling during dialysis: application to pediatric hemodialysis, Aritif. Kidney Dial. 18 (1995) 122–129.
[26] D. Schneditz, B. Fariyike, R. Osheroff, M.W. Levin, Is intercompartmental urea clearance during hemodialysis a perfusion term? A comparison of two pool urea kinetic models, J. Am. Soc. Nephrol. 6 (1995) 1360–1370.
[27] R.M. Hakim, T.A. Depner, T.F. Parker, Adequacy of hemodialysis, Am. J. Kidney Dis. 20 (1992) 108–122.
[28] T.A. Depner, Prescribing Hemodialysis, Kluwer Academic Publishers, New York, 1991, pp. 91–126.
[29] F.A. Gotch, Kinetic modeling in hemodialysis, in: A.R. Nissenson, R.N. Fine, D. Gentile (Eds.), Clinical Dialysis, Appleton and Lange, Norwalk, 1990, pp. 118–146.
[30] in: F. Lopot (Ed.), Urea Kinetic Modeling: EDTA/ERCA Series, vol. 4, D. Verlinde, Belgium, 1990.
[31] S. Pastan, C. Colton, Transcellular urea gradients cause minimal depletion of extracellular, during hemodialysis, ASAIO Trans. 35 (1989) 247–250.
[32] Z. Liao, C.K. Poh, Z. Huang, P.A. Hardy, W.R. Clark, D. Gao, A numerical and experimental study of mass transfer in the artificial kidney, J. Biomech. Eng. 125 (4) (2003) 472–480.
[33] C. Gostoli, A. Gatta, Mass transfer in a hollow fiber dialyzer, J. Membr. Sci. 6 (1980) 133–148.
[34] T.H. Maren, Chemistry of the renal reabsorption of bicarbonate, Can. J. Physiol. Pharmacol. 52 (1974) 1041.
[35] J. Gutknecht, M.A. Bisson, F.C. Tosteson, Effects of carbon anhydrase, bicarbonate and unstirred layers, J. Gen. Physiol. 69 (1977) 779–794.
[36] Z. Palaty, H. Bendova, Modeling and numerical analysis of counter-current dialyzer at steady state, Chem. Eng. Process. 49 (2010) 29–34.
[37] S.R. Suchdeo, J.S. Schultz, The permeability of gases through reacting solutions: the carbon dioxide-bicarbonate membrane system, Chem. Eng. Sci. 29 (1974) 13–23.
[38] N.V. Bhagavan, Medical Biochemistry, 4th ed., Jones & Bartlett Publishers, Boston, MA, 1992.
[39] Y. Moussy, Bioartificial kidney. Theoretical analyses of convective flow in hollow fiber modules: application to a bioartificial hemofilter, Biotechnol. Bioeng. 68 (2) (2000) 142–152.
[40] Y. Moussy, A.D. Snider, Laminal flow over pipe with injection and suction through the porous wall at low reynolds number, J. Membr. Sci. 327 (2009) 104–107.
[41] A. Frank, G. Lipscomb, M. Dennis, Visualization of concentration fields in hemodialyzers by computed tomography, J. Membr. Sci. 175 (2000) 239–251.
[42] M. Bossola, S. Giungi, L. Tazza, G. Luciani, Long-term oral sodium bicarbonate supplementation does not improve serum albumin levels in hemodialysis patients, Nephron Clin. Pract. 106 (2007) c51–c56.
[43] H.K. Versteeg, W. Malalasekera, An Introduction to Computational Fluid Dynamics—The Finite Volume Method, Longman Scientific and Technical, Harlow, UK, 1995.
[44] F.J. Gennari, Acid–base considerations in end-stage renal disease, in: W.L. Henrich (Ed.), Principles and Practice of Dialysis, 2nd ed., Williams and Wilkins, Baltimore, 1999, pp. 256–341.

[45] J. Lu, W.Q. Lu, A numerical simulation for mass transfer through the porous membrane of parallel straight channels, Int. J. Heat Mass Transfer 53 (2010) 2404–2413.
[46] S. Eloot, D.D. Wachter, I.V. Tricht, P. Verdonck, Computational flow modeling in hollow-fiber dialyzer, Artif. Organs 26 (7) (2002) 590–599.
[47] S. Tong, F. Yuan, An equivalent length model of microdialysis sampling, J. Pharm. Biomed. Anal. 28 (2002) 269–278.
[48] S. Eloot, P. Verdonck, Modeling of transport phenomena in an artificial kidney, in: Wiley Encyclopedia of Biomedical Engineering, John Wiley & Sons, New York, 2006, pp. 1444–1476.
[49] T. Symreng, M.J. Flanigan, V.S. Lim, Ventilatory and metabolic changes during high efficiency hemodialysis, Kidney Int. 41 (1992) 1064–1069.
[50] J. Uribarri, M. Zia, J. Mahmood, R.A. Marcus, Oh MS: acid production in chronic hemodialysis patients, J. Am. Soc. Nephrol. 9 (1998) 114–120.
[51] F.J. Gennari, Acid–base balance in dialysis patients, Semin. Dial. 13 (4) (2000) 235–239.
[52] L.A. Pedrini, V. De Cristofaro, B. Pagliari, Effects of the infusion mode on bicarbonate balance in on-line hemodiafiltration, Int J. Artif. Organs 25 (2) (2002) 100–106.
[53] A. Santoro, M. Spongano, G. Ferrari, et al., Analysis of the factors influencing bicarbonate balance during acetate free biofiltration, Kidney Int. 43 (Suppl. 41) (1993) S184–S187.
[54] P. Ahrenholz, R.E. Winkler, W. Ramlow, M. Tiess, O. Thews, Online hemodiafiltration with pre- and post-dilution: impact on the acid–base status, Int. J. Artif. Organs 21 (6) (1998) 321–327.
[55] A.J. Williams, I.D. Dittmer, A. McArley, J. Clark, High bicarbonate dialysate in haemodialysis patients: effects on acidosis and nutritional status, Nephrol. Dial. Transplant. 12 (12) (1997) 2633–2637.